A Robust Model Predictive Current Closed-Loop Control With Parameter Estimation Strategy Based on Immune Chaotic Antipredator PSO for PMSM

Yang Zhang, Sicheng Li, Wenjing Yi, Yiping Yang, Kun Cao, and Bing Luo

***Abstract*—Aiming at the issues of the current fluctuation and dependence of the control performance on model parameters accuracy in model predictive current control (MPCC) for a permanent magnet synchronous motor (PMSM), a robust model predictive current closed-loop control strategy with multiparameter estimation based on immune chaotic antipredator particle swarm optimization (RMPCC-ICAPSO) algorithm is proposed. The motor parameters are estimated by the ICAPSO algorithm and updated parameters are fed into the prediction model in real time. To begin with, the different single-phase voltage vectors are selected to synthesize the reference voltage vector, and the zero vector is split equally for redistribution. In addition, the immune chaotic theory is employed in updating the population of the PSO algorithm, learning factors as well as inertia weights. The ability of the algorithm to explore potentially better regions is enhanced, the problem of the local optimality is escaped, and the particle prematurity is suppressed. Moreover, an antipredator algorithm is introduced to the PSO, the worst solution position is excluded, the more uncharted regions are explored, and optimization of search accuracy is further enhanced. Finally, the RMPCC-ICAPSO strategy is experimentally demonstrated with a 3-kW motor. The correctness and effectiveness of the proposed RMPCC-ICAPSO strategy are proved by the experimental results.**

***Index Terms*—Immune chaotic antipredator particle swarm optimization (ICAPSO) algorithm, model predictive current control (MPCC), parameter estimation, permanent magnet synchronous motor (PMSM).**

I. Introduction

RECENTLY, the permanent magnet synchronous motor (PMSM) has been widely researched and applied in the field of rail transportation, electric vehicles, and ship electric [1], [2], [3] due to its advantages of high efficiency, high power density, and high reliability [4], [5]. To satisfy the control requirements of PMSM systems in the field of the electrical power industry, various strategies with unique advantages have been proposed. The field-oriented control strategy [6] is excellent in the steady state, but deficient in the dynamic response. Although the direct torque control strategy improves the response speed, it also causes issues such as unstable switching frequency, large transient torque ripples, and high current harmonic content [7]. Therefore, exploring effective strategies to improve the performance of PMSM is of great significance. The model predictive control is widely used in motor drive control due to its excellent characteristics such as rapid dynamic response and the ability to effectively address complex nonlinear constraints [8], [9]. However, the predictive control also has issues such as current harmonics and torque pulsations [10], [11], the predictive control algorithm relies on an accurate mathematical model, and the performance of the PMSM system is affected by the mismatch of the model parameters [12], [13].

A. Related Research

Nowadays, various research has been carried out by scholars to improve the robustness of predictive control algorithms and reduce the effects of parameter mismatch on the control performance of PMSM systems as much as possible. In [14], a novel robust MPCC strategy considering the effect of dynamic response is proposed. To begin with, the current error-based data acquisition methods for stator inductance and magnetic flux linkage are given. In addition, the accurate motor parameters are calculated by the proposed data acquisition method and compensated into the prediction model in real time. The effects caused by parameter mismatch are effectively eliminated by the acquisition method, and the robustness of the PMSM system is enhanced. In [15], an improved MPCC based on an incremental model is proposed. To begin with, an incremental prediction model is introduced, in which the use of flux linkage is eliminated in the prediction model. Furthermore, to improve the parameter interference resistance of the MPCC, an inductive interference control strategy is proposed, which includes an inductive interference observer and an inductor extraction algorithm. The accurate inductance information of the whole control system is updated in real time. In [16], a novel finite control set model predictive control is proposed. The evaluation of motor speed and stator current control objectives is accomplished by the

Received 11 March 2024; revised 12 July 2024; accepted 29 September 2024. Date of publication 8 October 2024; date of current version 12 December 2024. This work was supported in part by the National Natural Science Foundation of China under Grant 51907061 and in part by the Key Research and Development Program of Hunan Province of China under Grant 2023GK2006. Recommended for publication by Associate Editor J. Hur. *(Corresponding author: Yang Zhang.)*

Yang Zhang, Sicheng Li, Wenjing Yi, Yiping Yang, and Kun Cao are with the College of Electrical and Information Engineering, Hunan University of Technology, Zhuzhou 412007, China (e-mail: hut_zy@hut.edu.cn; lisicheng@stu.hut.edu.cn; yiwenjing@stu.hut.edu.cn; yangyiping@stu.hut.edu.cn; caokun@stu.hut.edu.cn).

Bing Luo is with the CSG Electric Power Research Institute Company Ltd., Guangzhou 510630, China (e-mail: luobing@csg.cn).

Color versions of one or more figures in this article are available at https://doi.org/10.1109/TPEL.2024.3476118.

Digital Object Identifier 10.1109/TPEL.2024.3476118

proposed strategy in the objective cost function and the structure of the control system is improved by closed-loop compensation. In [17], a robust two-vector MPCC based on the stator inductance extraction algorithm and flux linkage extraction algorithm is proposed and accurate inductance and flux linkage information is obtained in real time. In addition, the proportional-integral regulator parameters of extraction algorithms are theoretically derived. In [18], a robust MPCC with high computational efficiency is proposed. To begin with, the deadbeat predictive control is introduced to compute the reference voltage vector (RVV). According to the position of RVV to determine the optimal voltage vector, the number of iterations for selecting the voltage vector is reduced and the computational efficiency is improved. In addition, to reduce the sensitivity of the motor parameters, a parameter extraction strategy based on sliding mode observer is designed, and the parameter robustness of the MPCC is enhanced.

The observer is an effective strategy commonly used to compensate for concentrated disturbances. The basic principle is to synthesize all the influencing factors such as motor parameter mismatch and external disturbances into the total disturbance amount. The objective of the observer system is to estimate the total disturbance in real time to realize dynamic compensation. The observer can effectively reduce the effects of various disturbances on the system performance and improve the stability and accuracy of the control system. In [19], a real-time MPCC based on the exact model-aid extended state observer compensation strategy is proposed. This strategy converts the predictive controller into the form of multiparameter dual program and solves it by numerical computational strategies. In [20], an improved integral sliding mode control (IISMC) based on novel variable rate reaching law (NVRRL) and adaptive reduced order proportional integral observer (AROPIO) is proposed. The system state jitter and convergence time are simultaneously reduced by the NVRRL. To further enhance the tracking accuracy and anti-interference capability of the PMSM system, an AROPIO is designed to estimate set disturbances and provide feedforward compensation for IISMC. In [21], an active-disturbance-rejection sliding-mode current control (ADR-SMCC) strategy is proposed. The control law of SMCC is updated in real time with estimated internal disturbances. The robustness of the transient state is improved by the ADR-SMCC strategy.

Several scholars have researched parameter estimation strategies to compensate for PMSM parameter mismatch. The accurate estimation of motor parameters is obtained and the estimation of parameters is fed back into the prediction model. The control performance of the motor is improved and the operation efficiency is enhanced. In [22], an adjustable model predictive control strategy is proposed. The strategy employs an improved model-reference adaptive system to identify parameters online, the constant parameters are replaced by the identification parameters, and the identification parameters are fed back into the prediction model. The identification accuracy is improved and the robustness is enhanced. In [23], a long-term memory recursive least squares estimation strategy is proposed. The magnet flux linkage and differential inductance required for online self-adjustment are quickly identified. The transient performance of the predictive control strategy is improved. In [24], an improved particle swarm optimization strategy based on the Gaussian distribution model is proposed. The Gaussian individual optimal distribution is introduced by the algorithm and real-time updating of particle positions is realized. In [25], an incremental MPCC strategy with online parameter mismatch compensation is proposed. The model for incremental current prediction is established from the strategy, and the rotor magnetic flux linkage is eliminated. In addition, the linear relation is identified by the recursive least squares method with a forgetting factor, and the parameter mismatch of PMSM systems is compensated online. In [26], an improved deadbeat predictive current control strategy for interior PMSM based on parameter identification is proposed. The predictive control strategy observes the inductance and resistance values of interior PMSM online and replaces the initial parameters with identified parameters. In [27], an online multiparameter identification strategy is proposed which is able to identify inductance error, resistance error, magnet flux linkage, and equivalent magnitude of voltage distortion caused by inverter nonlinearity. In [28], a contraction factor antipredator PSO algorithm is proposed. The issues of algorithm falling into local optimization are overcome. However, the accuracy of the estimates needs to be further improved.

B. Motivation and Innovation

To solve the issues of current fluctuation and control performance dependent on model parameters in model predictive current control (MPCC) strategy for PMSM, a robust model predictive current closed-loop control strategy with parameter estimation based on immune chaotic antipredator particle swarm optimization (RMPCC-ICAPSO) algorithm is proposed. The motor parameters are estimated by the proposed ICAPSO algorithm and the updated parameters are fed into the prediction model in real time. To begin with, the different voltage vectors are selected to synthesize the RVV, and the zero vector is split equally for redistribution. In addition, the immune chaotic theory is employed in the updating of PSO algorithm populations, and learning factors. The ability of the algorithm to explore potentially better areas is enhanced, the problem of the local optimality is escaped, and the particle prematurity is suppressed. Finally, an antipredator algorithm is introduced to the particle swarm optimization, the more uncharted areas are explored, and the optimization search accuracy is further enhanced.

C. Paper Organization

The rest of the sections are organized as follows. The description of the mathematical model and parameter estimation model for PMSM is introduced in Section II. The theoretical analysis of conventional predictive current control with parameter estimation is described in Section III. The design of the robust MPCC strategy with parameter estimation based on the immune chaotic antipredator PSO algorithm is described in Section IV. The experimental verification and comparative analysis are described in Section V. Finally, Section VI concludes this article.

II. Description of the Mathematical and Parameter Estimation Model for PMSM

A. Mathematical Model of PMSM

The mathematical model of the PMSM is established using the synchronous rotating coordinate system [29]. The dynamic equation of stator voltage is expressed as

$$\begin{cases} u_d = R_s i_d + L_d \frac{di_d}{dt} - \omega_e L_q i_q \\ u_q = R_s i_q + L_q \frac{di_q}{dt} + \omega_e L_d i_d + \omega_e \psi_f \end{cases} \tag{1}$$

where u_d and u_q represent the dq-axis voltage, i_d and i_q represent the dq-axis current, L_d and L_q represent the dq-axis stator inductance, and R_s, ω_e, and ψ_f represent the stator resistance, electromagnetic rotation angle, and magnet flux linkage, respectively.

The equation for the dq-axis flux linkage is expressed as

$$\begin{cases} \psi_d = L_d i_d + \psi_f \\ \psi_q = L_q i_q \end{cases}. \tag{2}$$

The equation for the electromagnetic torque is expressed as

$$T_e = \frac{3}{2} n_p i_q \left[\psi_f + (L_d - L_q) i_d\right] \tag{3}$$

where n_p represents the pole pair number.

B. Design of Parameter Estimation Model

In the steady-state case, the discrete voltage equation is expressed as

$$\begin{cases} u_d(k) = R_s i_d(k) - \omega_e(k) L_q i_q(k) \\ u_q(k) = R_s i_q(k) + \omega_e(k) L_d i_d(k) + \omega_e(k) \psi_f \end{cases}. \tag{4}$$

The parameters to be identified are R_s, L_d, L_q, and ψ_f. The voltage equation in (4) is of order 2, and the equation is in an underranked state, which causes the algorithm to misconverge and the recognition results to be inaccurate [30].

To solve the problem of underranking between the order of equation and estimated parameter, the instantaneous input of negative-order d-axis current, the full-rank discrete equation of the dq-axis of the motor is expressed as

$$\begin{cases} u_{d0}(k) = -\omega_e(k) L_q i_{q0}(k) \\ u_{q0}(k) = R_s i_{q0}(k) + \omega_e(k) \psi_{f0} \\ u_d(k) = R_s i_d(k) - \omega_e(k) L_q i_q(k) \\ u_q(k) = R_s i_q(k) + \omega_e(k) L_d i_d(k) + \omega_e(k) \psi_f \end{cases} \tag{5}$$

where the subscript 0 denotes variables and parameters under $i_d = 0$ control, and the rest denotes variables and parameters under $i_d < 0$ control.

III. Theoretical Analysis of Predictive Current Control With Parameter Estimation Strategy

A. Conventional MPCC Strategy

The objective of conventional MPCC strategy is to ensure that the current accurately tracks its reference value, to achieve accurate control of the system and to optimize the dynamic response [31].

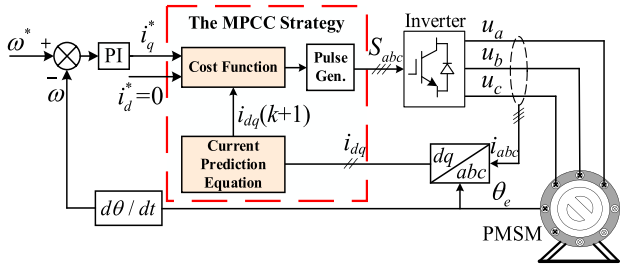

Fig. 1. Control diagram of the conventional MPCC strategy.

According to the forward Euler equation, the mathematical description of discrete current prediction is expressed as

$$\begin{cases} i_d(k+1) = i_d(k) - \frac{R_s T_k}{L_d} i_d(k) + \frac{L_q T_k}{L_d} \omega_e(k) i_q(k) \\ \qquad + \frac{T_k}{L_d} u_d(k) \\ i_q(k+1) = i_q(k) - \frac{R_s T_k}{L_q} i_q(k) - \frac{L_d T_k}{L_q} \omega_e i_d(k) \\ \qquad - \frac{\psi_f T_k}{L_q} \omega_e(k) + \frac{T_k}{L_q} u_q(k) \end{cases} \tag{6}$$

where T_k represents the control period of the PMSM system.

According to (6), the model predictive control algorithm predicts the stator current response under the action of eight fundamental voltage vectors [32]. The prediction results are integrated into the objective function and traversal optimization is performed to determine the optimal voltage vector. The objective function of the predictive current control strategy is shown in the following equation:

$$g = \left|i_d(k+1) - i_d^*\right|^2 + \left|i_q(k+1) - i_q^*\right|^2 \tag{7}$$

where i_d^* and i_q^* are represented as the references of current in the dq-axis. The control diagram of MPCC is shown in Fig. 1.

The conventional predictive control strategy iteratively computes multiple discrete vectors based on the cost function. However, the computational complexity of the predictive controllers increases exponentially as the voltage level increases [33]. In addition, the discrete characteristics of the predictive model impose limitations on the selection of voltage vectors. It can only select outputs from the predefined finite set of voltage vectors, thus continuous amplitude and phase regulation cannot be achieved [34].

B. Description of the MPCC Based on Deadbeat Principle

As the complexity of an inverter increases, the computational burden on the predictive controller increases exponentially. However, closed-loop control of the inverter output voltage can be achieved by the deadbeat principle. The reference voltage value is continuously adjusted according to the real-time voltage error conditions to achieve the desired output control objective.

According to the deadbeat principle, the reference voltage values u_d^* and u_q^* at the next time is expressed as

$$\begin{cases} u_d^* = \frac{L_d}{T_k}\left[i_d^* - \left(1 - \frac{R_s T_k}{L_d}\right) i_d(k) - \frac{L_q T_k \omega_e(k) i_q(k)}{L_d}\right] \\ u_q^* = \frac{L_q}{T_k}\left[i_q^* - \left(1 - \frac{R_s T_k}{L_q}\right) i_q(k) \right. \\ \qquad \left. + \frac{L_d T_k \omega_e(k) i_d(k)}{L_q} + \frac{T_k \psi_f \omega_e(k)}{L_q}\right] \end{cases}. \tag{8}$$

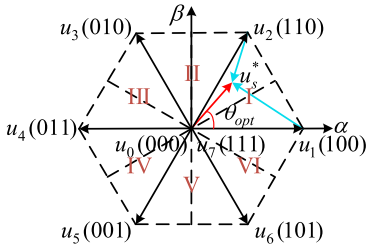

Fig. 2. Diagram of the synthesized voltage vector and the distribution of the phase voltage vectors.

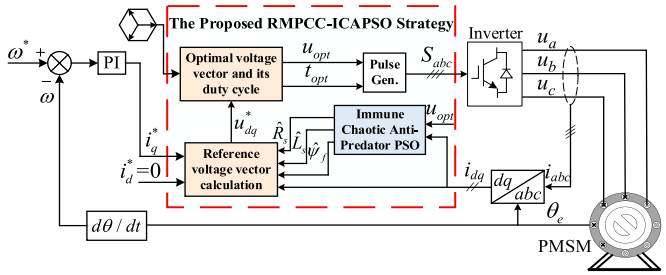

Fig. 3. Control diagram of the proposed robust model predictive current control strategy based on immune chaotic antipredator PSO algorithm.

According to the transform of dq-$\alpha\beta$, u_d^* and u_q^* are converted to u_α^* and u_β^* as shown in the following equation:

$$\begin{cases} u_\alpha^* = u_d^* \cos(\theta_e) - u_q^* \sin(\theta_e) \\ u_\beta^* = u_d^* \sin(\theta_e) + u_q^* \cos(\theta_e) \end{cases}. \tag{9}$$

The RVV is selected by means of the diagram of voltage space vector positions. The diagram of the synthesized voltage vector and the distribution of the phase voltage vectors are shown in Fig. 2.

$$\begin{cases} u_s^* = u_\alpha^* + i u_\beta^* \\ \theta_{\text{opt}} = \arctan u_\beta^* / u_\alpha^* \end{cases} \tag{10}$$

where θ_{opt} is the angle of the α-axis with the reference voltage and i is the imaginary unit.

However, the fundamental voltage vector for the MPCC exhibits fixed amplitude and phase characteristics. The voltage vector selection with a fundamental voltage vector leads to imprecision and affects the performance of the control system.

C. Basic Principle of PSO Algorithm

The PSO algorithm is a stochastic evolutionary iterative optimization algorithm, which is based on the artificially designed fitness function to evaluate the quality of the information currently carried by the particles, to guide the particles to move toward a higher-quality position, and ultimately reach the optimal solution [35].

The key to the PSO algorithm is the particle velocity and position update formula, which is continuously updated with the increase of the iteration number to approach the optimal solution step by step. The update equation is described as

$$\begin{cases} v_{i_d}^{k+1} = \omega v_{i_d}^k + c_1 r_1 (P_{\text{best}} - x_{i_d}^k) + c_2 r_2 (G_{\text{best}} - x_{i_d}^k) \\ x_{i_d}^{k+1} = x_{i_d}^k + v_{i_d}^{k+1} \end{cases} \tag{11}$$

where v_{i_d} and x_{i_d} are velocity and position of the particle i, P_{best} is the optimal position, G_{best} is the global best position of the whole particle swarm, and ω is inertia weight. c_1 and c_2 are learning factors and r_1 and r_2 are random numbers between 0 and 1. The superscripts k and $k+1$ denote iterations k and $k+1$, respectively.

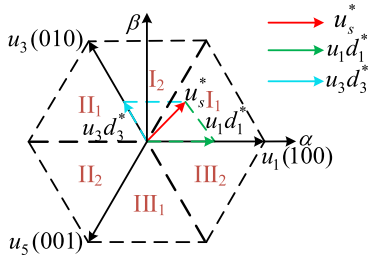

Fig. 4. Schematic of the synthesized reference voltage vector.

IV. Design of the Robust MPCC Strategy With Parameter Estimation Based on Immune Chaotic Antipredator PSO Algorithm

The conventional MPCC belongs to the open-loop control. When the parameters employed in model predictive equations are mismatched, the prediction model cannot be adjusted quickly and the accuracy of predictive control will be affected. In addition, the predictive control strategy cannot realize accurate control of current due to external disturbances and other problems.

In the research, a robust model predictive current closed-loop control strategy with parameter estimation based on the ICAPSO algorithm is proposed. To begin with, the three different single-phase voltage vectors with a spatial difference of 120° are selected to synthesize the RVV and the zero vector is split equally for redistribution. In addition, the immune chaotic theory is employed in updating the population of the PSO algorithm, learning factors as well as inertia weights. The issue of the local optimality is escaped and the particle prematurity is proposed. Moreover, an antipredator PSO algorithm is added, the worst solution position is excluded, the more uncharted areas are explored, and optimization of search accuracy is further enhanced. The control diagram of the proposed robust MPCC strategy based on the immune chaotic antipredator PSO algorithm is shown in Fig. 3.

A. Design of the Robust Model Predictive Current Closed-Loop Control

In Fig. 4, the three different single-phase voltage vectors with a spatial difference of 120° are selected in the research to delineate the whole hexagon. The RVV u_s can be synthesized by the single-phase voltage vectors u_1 and u_3 whenever it is

located in any sector. The synthesized RVV u_s is expressed as

$$u_s^* = u_1 d_1^* + u_3 d_3^* \tag{12}$$

where u_1 and u_3 represent the phase voltage vectors and d_1^* and d_3^* represent the duty cycle of u_1 and u_3.

The dq-axis component of the synthesized RVV is expressed as

$$\begin{cases} u_d = u_{1d} d_1^* + u_{3d} d_3^* \\ u_q = u_{1q} d_1^* + u_{3q} d_3^* \end{cases} \tag{13}$$

where $u_{1x}(x = d, q)$ represents the component of u_1 and u_{3x} represents the component of u_3.

According to (6) and (13), the stator current is controlled with the deadbeat principle and the duty cycles of u_1 and u_3 are expressed as

$$\begin{cases} d_1^* = \frac{(s_{\psi d} + R_s i_d(k) + e_d(k)) u_{3q}}{u_{1d} u_{3q} - u_{1q} u_{3d}} - \frac{(s_{\psi q} + R_s i_q(k) + e_q(k)) u_{3d}}{u_{1d} u_{3q} - u_{1q} u_{3d}} \\ d_3^* = \frac{s_{\psi d} + R_s i_d(k) + e_d(k) - u_{1d} d_1^*}{u_{3d}} \end{cases} \tag{14}$$

where $s_{\psi d} = L_d \frac{i_d(k+1) - i_d(k)}{T_k}$, $s_{\psi q} = L_q \frac{i_q(k+1) - i_q(k)}{T_k}$, $s_d = R_s i_d(k) + e_d(k)$, and $s_q = R_s i_q(k) + e_q(k)$.

According to the above analysis, the three-phase duty cycle is calculated as follows.

1) When $d_1{}^* > 0$ and $d_3{}^* > 0$, $d_a = -d_1{}^*$, $d_b = d_3{}^*$, and $d_c = 0$.
2) When $d_1{}^* < 0$ and $d_3{}^* - d_1{}^* > 0$, $d_a = 0$, $d_b = d_3{}^* - d_1{}^*$, and $d_c = -d_1{}^*$.
3) When $d_3{}^* < 0$ and $d_3{}^* - d_1{}^* < 0$, $d_a = d_1{}^* - d_3{}^*$, $d_b = 0$, and $d_c = -d_3{}^*$.

The performance of the PMSM is further improved if the zero vector is equally assigned to u_0 and u_7. Define the duty cycle of the zero vector as

$$d_0 = 1 - \max\left[d_a, d_b, d_c\right]. \tag{15}$$

Then the duty cycle of u_7 is expressed as

$$d_{u7} = \frac{1}{2}\left(1 - \max\left[d_a, d_b, d_c\right]\right). \tag{16}$$

The duty cycle is expressed as

$$\begin{cases} d_a^* = d_a + d_{u7} \\ d_b^* = d_b + d_{u7} \\ d_c^* = d_c + d_{u7}. \end{cases} \tag{17}$$

The duty cycle d_a^*, d_b^*, and d_c^* maybe out of the range [0 1] as the load torque and rotation speed of the motor change suddenly: at this point, further corrections are required. If the duty cycle of any phase is negative, it is set to 0; if the duty cycle is more than 1, it is reassigned.

Taking the example of d_a^* more than 1, the reassigned duty cycle d_a^*, d_b^*, and d_c^*can be expressed as

$$\begin{cases} d_a^* = 1 \\ d_b^* = d_b^* / d_a^* \\ d_c^* = d_c^* / d_a^* \end{cases}. \tag{18}$$

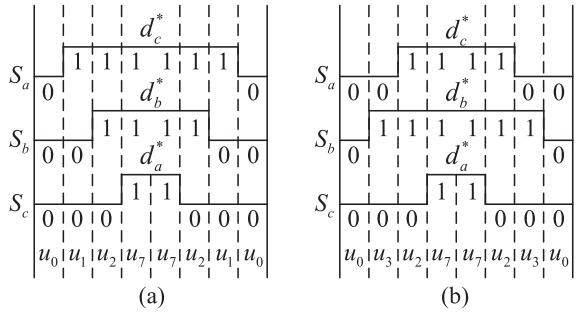

Fig. 5. Diagram of the three-phase duty cycle. (a) u_s^* is located in sector I_1. (b) u_s^* is located in sector I_2.

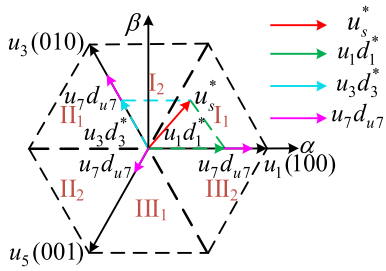

Fig. 6. Synthetic diagram of the synthesized reference voltage vector u_s^*.

The diagram of the duty cycle of sectors I_1 and I_2 after equalizing the zero vector is shown in Fig. 5.

The schematic of the synthesized RVV u_s^* of the robust model predictive current closed-loop control strategy with parameter estimation based on the immune chaotic antipredator PSO algorithm is shown in Fig. 6.

B. Design of the Immune Chaotic Antipredator Particle Swarm Optimization Algorithm

Antipredator strategies exist in nature, for example, in groups of animals foraging for food. To avoid encounters with natural enemies, the antipredator PSO algorithm combines and transmits information about the optimum food location and location of natural enemy encounters within the population. If one individual discovers a natural enemy, the other individuals will avoid encountering natural enemies, and the probability of predation is diminished.

The PSO algorithm's individual cognitive part is divided into two components: the memory of the particle's best position and the particle's worst position. The social experience of the PSO is divided into the global worst and best experiences. Then, according to (11), the equation for the antipredator PSO algorithm can be rewritten as

$$\begin{cases} v_{id}^{k+1} = \omega v_{id}^k + c_1 r_1 (P_{\text{best}}^k - x_{id}^k) + c_3 r_3 (x_{id}^k - P_{\text{worst}}^k) \\ \qquad\quad + c_2 r_2 (G_{\text{best}}^k - x_{id}^k) + c_4 r_4 (x_{id}^k - G_{\text{worst}}^k) \\ x_{id}^{k+1} = x_{id}^k + v_{id}^{k+1} \end{cases} \tag{19}$$

where c_1 and c_3 are the acceleration coefficients of particles flying toward the best position and away from the poorest position of the individual, respectively. c_2 and c_4 are the acceleration coefficients of particles flying toward the best position and away from the poorest position of the population, respectively.

The chaotic algorithm is improved by adjusting the position information of the particles [36]. The improved position equation is expressed as

$$x_{i_d}^{k+1} = x_{i_d}^k + z^{k+1}(x_{id\max}^k - x_{id\min}^k) \tag{20}$$

where $x_{id\max}^k$ and $x_{id\min}^k$ are maximum and minimum values of particles occurring during the iteration, respectively. Z^{k+1} is a random number between 0 to 1.

When the algorithm falls into a local optimization, a criterion needs to be given to determine whether the local optimization is reached. The adaptation variance of the population is set as the reference value, which is expressed as

$$\sigma^2 = \frac{1}{n}\left(\frac{f_i - f_{\text{average}}}{f}\right)^2 \tag{21}$$

where n is the total number of particles, σ^2 is the population fitness, f_i is the fitness of the ith particle, $f_{average}$ is the average fitness of the population, and f is the constraint factor.

The immune algorithm is improved by incorporating a novel immune upgrade strategy. The improved particle position equation is expressed as

$$x_{i_d}^{k+1} = x_{i_d}^k - r_1(x_{i_d}^k - G_{\text{best}}) + r_2 x_{i_d}^k \text{Cauchy} \tag{22}$$

where $x_{i_j}^{k+1}$ represents the position of particle in real time and Cauchy represents standard Cauchy distribution.

The inertia weight affects the global and local optimization of the algorithm as well as the ability of the algorithm to find the optimal value. The designed inertia weight is expressed as

$$\omega = (\omega_{\max} - \omega_{\min})e^{-(\tau\frac{t^k}{t_{\max}})^2} + \omega_{\min} \tag{23}$$

where $\omega_{\max}$ and $\omega_{\min}$ are upper and lower bounds of the inertia weight values, τ is the empirical factor, and t^k and $t_{\max}$ are the current and maximum number of iterations.

The steps for the identification of the immune chaotic antipredator PSO are shown as follows.

Step 1: The system generates a random population and initializes parameters such as t, c_1, c_2, c_3, c_4, ω, $v_{i_d}^k$, and $x_{i_d}^k$.

Step 2: The initial local optimum P_{best}^k and the initial global optimum G_{best}^k are obtained from the fitness function.

Step 3: The position and velocity information of the particles are updated through (19).

Step 4: The adaptation variance is calculated according to (21) and compared with the variance threshold, if it is less than the latter then go to Step 6, otherwise go to Step 5.

Step 5: The new particle parameters are obtained by chaotic processing of the particle positions according to (20).

Step 6: All particles are sorted according to the fitness value. Individuals located in the middle 1/4 are updated by (22).

Step 7: When the number of iterations reaches the set value, the global optimal solution is obtained and the iteration is stopped, otherwise go to Step 3.

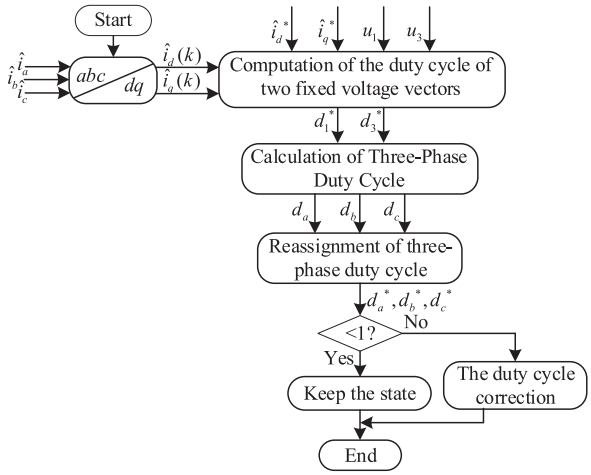

Fig. 7. Schematic of PMSM parameter estimation.

C. Design of Parameter Estimation Model Based on the Proposed Immune Chaotic Antipredator PSO Algorithm

The flowchart of the robust MPCC algorithm based on the parameter estimation strategy is shown in Fig. 7.

The principle of the parameter estimation is through the proposed immune chaotic antipredator PSO algorithm to continuously correct the parameters to be recognized in the adjustable model until the value of the fitness function tends to 0.

The optimal solution obtained by the system is used as the recognized motor parameters. According to (6), the adjustable model is expressed as

$$\begin{bmatrix}\hat{i}_d(k+1)\\ \hat{i}_q(k+1)\end{bmatrix} = \begin{bmatrix}1-\frac{\hat{R}_s(k)T_k}{\hat{L}_d(k)} & \omega_e(k)\frac{\hat{L}_q(k)T_k}{\hat{L}_d}\\ -\omega_e(k)\frac{\hat{L}_d(k)}{\hat{L}_q(k)} & 1-\frac{\hat{R}_s(k)T_k}{\hat{L}_q(k)}\end{bmatrix}\begin{bmatrix}\hat{i}_d(k)\\ \hat{i}_q(k)\end{bmatrix} + \begin{bmatrix}\frac{T_k}{\hat{L}_d(k)} & 0\\ 0 & \frac{T_k}{\hat{L}_q(k)}\end{bmatrix}\begin{bmatrix}u_d(k)\\ u_q(k)-\omega_e(k)\hat{\psi}_f(k)\end{bmatrix}. \tag{24}$$

The similarity between the motor reference model and the adjustable model needs to be evaluated by designing the fitness function, which is defined as

$$f(R_s, L_d, L_q, \psi_f) = \left[i_d(k) - \hat{i}_d(k)\right]^2 + \left[i_q(k) - \hat{i}_q(k)\right]^2. \tag{25}$$

The schematic of PMSM parameter estimation is shown in Fig. 8. u_d, u_q, i_d, i_q, and ω_e are the outputs of the reference model. The output results are compared by means of fitness function, the reference model is continuously corrected by the ICAPSO algorithm, and the particle with the best position participates in the next iteration until the output is reached.

The steps of PMSM parameter estimation based on ICAPSO are set as follows.

Step 1: Set in control mode of $i_d = 0$, collect u_d, u_q, i_d, i_q, and ω_e and run them, saving several sets of data.

Step 2: Initialize the algorithm and all related parameters.

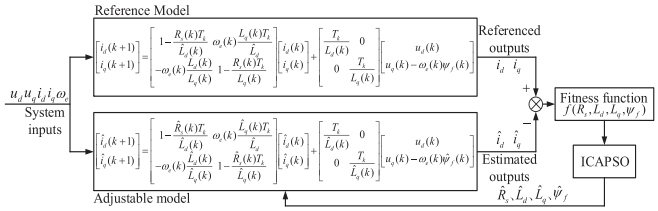

Fig. 8. Schematic diagram of PMSM parameter estimation based on ICAPSO algorithm.

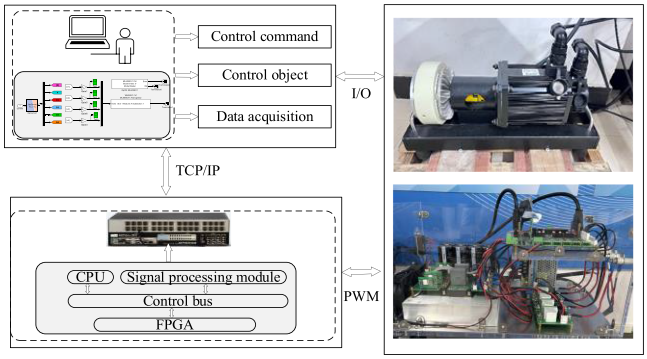

Fig. 9. Diagram of the physics experiment platform.

Step 3: Import the data into the algorithm. Iteratively update parameters according to the algorithm to get estimated values.

Step 4: The referenced values are obtained from the motor model.

Step 5: The new fitness function value is the sum of squares of the differences between the estimated and referenced values.

Step 6: According to the iterative law of the algorithm, the local optimum and global optimum are obtained by the comparison of the adapted value functions.

Step 7: Initial parameter estimated values are obtained and the most appropriate estimated values are selected through iterative experiments.

Step 8: Determine whether the requirements are met, if not continue to execute Step 3.

V. Experimental Verification

The hardware platform for the experiment is presented in Fig. 9. The experimental platform consists of a digital signal processor, PMSM, and a PWM inverter. The control frequency of the experiment is set to 10 kHz and the average switching frequency of the inverter is 10 kHz. The PMSM control parameters relevant to this context are supplied in Table I.

To verify the performance of the proposed robust MPCC strategy based on an improved immune chaotic antipredator PSO algorithm, the following parameters conditions are set as: a) $R = 0.5R_s$ and $\psi_f = 0.5\psi_{f0}$; b) $R = 1.5R_s$ and $\psi_f = 1.5\psi_{f0}$; c) $R = 0.5R_s$, $\psi_f = 0.5\psi_{f0}$, and $L_s = 0.5L_{s0}$; and d) $R = 1.5R_s$, $\psi_f = 1.5\psi_{f0}$, and $L_s = 1.5L_{s0}$. The real-time estimated motor parameters are fed back to the prediction model. The experiments are organized as follows.

TABLE I
Parameters of PMSM Drive Systems

Parameter	Symbol	Value
Number of pole pairs	n_p	4
Stator inductance	L_s	1.625 mH
Stator resistance	R_s	0.22 Ω
Magnet flux linkage	ψ_f	0.1 Wb
DC voltage	U_{dc}	311 V
Rated torque	T_e	15 N·m
Rated speed	N	1000 r/min
Rated power	P_N	3 kW
Inertia	J	0.0048 kg·m^2

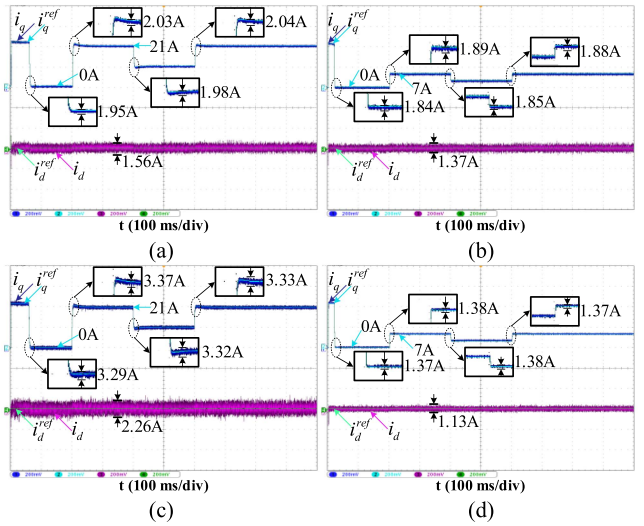

Fig. 10. Performance of the dq-axis current for the MPCC-CFAPSO strategy in [28]. (a) $R = 0.5R_s$ and $\psi_f = 0.5\psi_{f0}$. (b) $R = 1.5R_s$ and $\psi_f = 1.5\psi_{f0}$. (c) $R = 0.5R_s$, $\psi_f = 0.5\psi_{f0}$, and $L_s = 0.5L_{s0}$. (d) $R = 1.5R_s$, $\psi_f = 1.5\psi_{f0}$, and $L_s = 1.5L_{s0}$.

1) The RMPCC-ICAPSO is compared with the MPCC-CFAPSO in [28]. The proposed RMPCC-ICAPSO is verified to have better robust performance under parameter mismatch.
2) The RMPCC-ICAPSO is compared with the MPCC-DSCPSO in [36]. The proposed RMPCC-ICAPSO is verified to have better robust performance under parameter mismatch.

A. Performance of the dq-Axis Current Under Parameter Mismatch

To test the robustness of the RMPCC-ICAPSO strategy under parameter mismatch, the error motor parameters are used as the initial values. The erroneous motor parameters are estimated by the ICAPSO algorithm and estimated parameters are used in the RMPCC to replace the initial given parameters.

In Figs. 10–12, the performance results of the dq-axis current for RMPCC-ICAPSO, MPCC-CFAPSO, and MPCC-DSCPSO are shown under various conditions and parameters.

In Tables II and III, the performance of the three strategies is compared for transient state. The ripple of the dq-axis current is evaluated by the respective standard deviations σi_d and σi_q. The

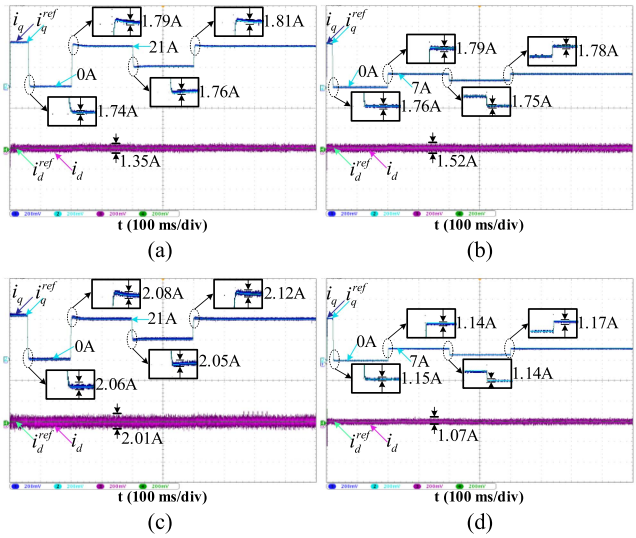

Fig. 11. Performance of the *dq*-axis current for the MPCC-DSCPSO strategy in [36]. (a) $R = 0.5R_s$ and $\psi_f = 0.5\psi_{f0}$. (b) $R = 1.5R_s$ and $\psi_f = 1.5\psi_{f0}$. (c) $R = 0.5R_s$, $\psi_f = 0.5\psi_{f0}$, and $L_s = 0.5L_{s0}$. (d) $R = 1.5R_s$, $\psi_f = 1.5\psi_{f0}$, and $L_s = 1.5L_{s0}$.

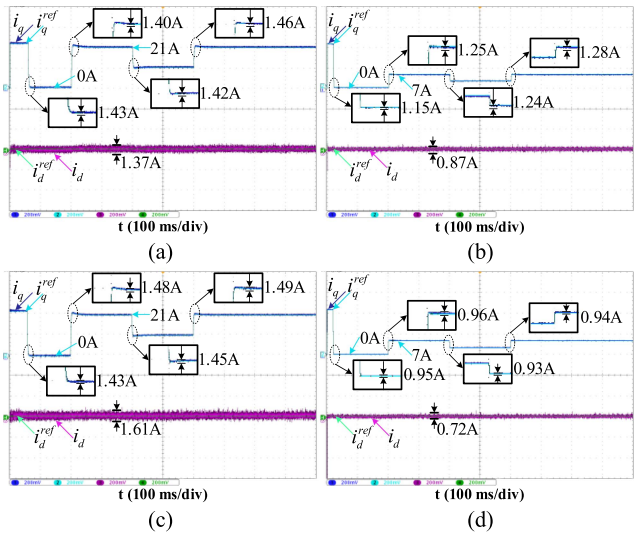

Fig. 12. Performance of the *dq*-axis current for the proposed RMPCC-ICAPSO strategy. (a) $R = 0.5R_s$ and $\psi_f = 0.5\psi_{f0}$. (b) $R = 1.5R_s$ and $\psi_f = 1.5\psi_{f0}$. (c) $R = 0.5R_s$, $\psi_f = 0.5\psi_{f0}$, and $L_s = 0.5L_{s0}$. (d) $R = 1.5R_s$, $\psi_f = 1.5\psi_{f0}$, and $L_s = 1.5L_{s0}$.

difference in average values of the reference and actual current is represented by the tracking error i_{d_error} and i_{q_error}.

In case of $R = 0.5R_s$ and $\psi_f = 0.5\psi_{f0}$, the proposed RMPCC-ICAPSO has σi_d of 1.1078 A, σi_q of 2.0936 A, i_{d_error} of 0.5924 A, and i_{q_error} of 0.8725 A. σi_d, σi_q, i_{d_error}, and i_{q_error} of the RMPCC-ICAPSO reduced by 19.44%, 21.67%, 22.38%, and 36.82%, respectively, compared to the MPCC-CFAPSO. σi_d, σi_q, i_{d_error}, and i_{q_error} of RMPCC-ICAPSO reduced by 16.48%, 15.81%, 19.03%, and 31.19%, respectively, compared to the MPCC-DSCPSO.

In case of $R = 0.5R_s$, $\psi_f = 0.5\psi_{f0}$, and $L_s = 0.5L_s$, the proposed RMPCC-ICAPSO has σi_d of 1.5062 A, σi_q of 2.2905 A, i_{d_error} of 0.7925 A, and i_{q_error} of 0.9825 A. σi_d, σi_q, i_{d_error}, and i_{q_error} of the RMPCC-ICAPSO reduced by 21.89%, 34.25%, 22.79%, and 55.72%, respectively, compared to MPCC-CFAPSO. σi_d, σi_q, i_{d_error}, and i_{q_error} of RMPCC-ICAPSO reduced by 14.87%, 17.85%, 19.60%, and 39.71%, respectively, compared to MPCC-DSCPSO.

TABLE II
COMPARISON OF PERFORMANCE OF MPCC-CFAPSO, MPCC-DSCPSO, AND RMPCC-ICAPSO UNDER PARAMETER REDUCTION

Parameter mismatch	Strategy	σi_d (A)	σi_q (A)	i_{d_error} (A)	i_{q_error} (A)
R=0.5R_s, ψ_f=0.5ψ_{f0}	MPCC-CFAPSO	1.3752	2.6715	0.7632	1.3809
	MPCC-DSCPSO	1.3264	2.4867	0.7316	1.2681
	RMPCC-ICAPSO	1.1078	2.0936	0.5924	0.8725
R=0.5R_s, ψ_f=0.5ψ_{f0}, L_s=0.5L_s	MPCC-CFAPSO	1.9283	3.4837	1.0264	2.2186
	MPCC-DSCPSO	1.7692	2.7882	0.9857	1.6296
	RMPCC-ICAPSO	1.5062	2.2905	0.7925	0.9825

In case of $R = 1.5R_s$ and $\psi_f = 1.5\psi_{f0}$, the proposed RMPCC-ICAPSO has σi_d of 0.8326 A, σi_q of 2.0635 A, i_{d_error} of 0.4256 A, and i_{q_error} of 0.8629A. σi_d, σi_q, i_{d_error}, and i_{q_error} of RMPCC-ICAPSO reduced by 29.99%, 17.67%, 35.24%, and 36.43%, respectively, compared to MPCC-CFAPSO. σi_d, σi_q, i_{d_error}, and i_{q_error} of the RMPCC-ICAPSO reduced by 26.95%, 6.32%, 33.48%, and 35.71%, respectively, compared to the MPCC-DSCPSO.

In case of $R = 1.5R_s$, $\psi_f = 1.5\psi_{f0}$, and $L_s = 1.5L_s$, the proposed RMPCC-ICAPSO has σi_d of 0.7169 A, σi_q of 1.3612 A, i_{d_error} of 0.3605 A, and i_{q_error} of 0.6078 A. σi_d, σi_q, i_{d_error}, and i_{q_error} of the RMPCC-ICAPSO reduced by 37.51%, 37.26%, 36.28%, and 44.43% compared to MPCC-CFAPSO. σi_d, σi_q, i_{d_error}, and i_{q_error} of RMPCC-ICAPSO reduced by 28.58%, 23.75%, 32.69%, and 23.39% compared to MPCC-DSCPSO.

B. Performance of the Motor Rotation Speed and the Electromagnetic Torque Under Parameter Mismatch

In Figs. 13–15, the motor speed ω_e and electromagnetic torque T_e of the RMPCC-ICAPSO, MPCC-CFAPSO, and MPCC-DSCPSO are shown under various conditions and parameters. The load torque increases from 0 to 8.0 N·m at 0.2 s, decreases to 4.0 N·m at 0.4 s and increases to 8.0 N·m at 0.6 s. The comparison of average motor speed response and torque ripple under parameter reduction is shown in Table IV and the comparison of average motor speed response and torque ripple under parameter increase is shown in Table V.

In case of $R = 0.5R_s$ and $\psi_f = 0.5\psi_{f0}$, the average speed response of RMPCC-ICAPSO is 0.0155 s, and the average torque ripple is 0.6127 N·m. The average speed response of RMPCC-ICAPSO is improved by 24.39% compared to the MPCC-CFAPSO, and improved by 9.88% compared to the MPCC-DSCPSO. The average torque ripple of RMPCC-ICAPSO is

TABLE III
COMPARISON OF PERFORMANCE OF MPCC-CFAPSO, MPCC-DSCPSO, AND RMPCC-ICAPSO UNDER PARAMETER INCREASE

Parameter mismatch	Strategy	σi_d (A)	σi_q (A)	i_{d_error} (A)	i_{q_error} (A)
R=1.5R_s, ψ_f=1.5ψ_{f0}	MPCC-CFAPSO	1.2179	2.5064	0.6572	1.3574
	MPCC-DSCPSO	1.1672	2.2027	0.6398	1.3422
	RMPCC-ICAPSO	0.8526	2.0635	0.4256	0.8629
R=1.5R_s, ψ_f=1.5ψ_{f0}, L_s=1.5L_s	MPCC-CFAPSO	1.1472	2.1695	0.5658	1.0938
	MPCC-DSCPSO	1.0038	1.7851	0.5356	0.7934
	RMPCC-ICAPSO	0.7169	1.3612	0.3605	0.6078

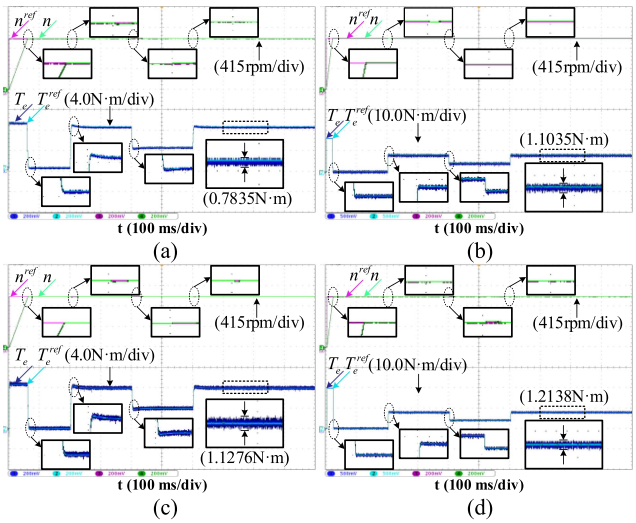

Fig. 13. Performance of the speed ω_e and torque T_e for the MPCC-CFAPSO strategy in [28]. (a) $R = 0.5R_s$ and $\psi_f = 0.5\psi_{f0}$. (b) $R = 1.5R_s$ and $\psi_f = 1.5\psi_{f0}$. (c) $R = 0.5R_s$, $\psi_f = 0.5\psi_{f0}$, and $L_s = 0.5L_{s0}$. (d) $R = 1.5R_s$, $\psi_f = 1.5\psi_{f0}$, and $L_s = 1.5L_{s0}$.

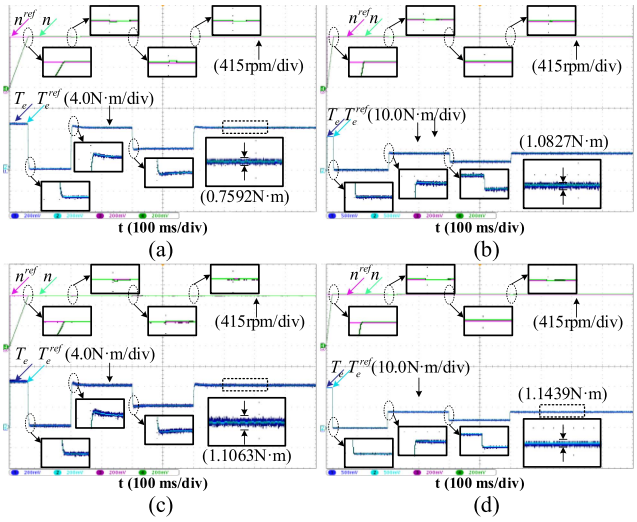

Fig. 14. Performance of the speed ω_e and torque T_e for the MPCC-DSCPSO strategy in [36]. (a) $R = 0.5R_s$ and $\psi_f = 0.5\psi_{f0}$. (b) $R = 1.5R_s$ and $\psi_f = 1.5\psi_{f0}$. (c) $R = 0.5R_s$, $\psi_f = 0.5\psi_{f0}$, and $L_s = 0.5L_{s0}$. (d) $R = 1.5R_s$, $\psi_f = 1.5\psi_{f0}$, and $L_s = 1.5L_{s0}$.

TABLE IV
COMPARISON OF AVERAGE MOTOR SPEED RESPONSE AND TORQUE RIPPLE UNDER PARAMETER REDUCTION

Parameter mismatch	Control strategy	Speed response (s)	Torque ripple (N·m)
R=0.5R_s, ψ_f=0.5ψ_{f0}	MPCC-CFAPSO	0.0205	0.7835
	MPCC-DSCPSO	0.0172	0.7592
	RMPCC-ICAPSO	0.0155	0.6127
R=0.5R_s, ψ_f=0.5ψ_{f0}, L_s=0.5L_s	MPCC-CFAPSO	0.0204	1.1276
	MPCC-DSCPSO	0.0173	1.1063
	RMPCC-ICAPSO	0.0158	0.8409

TABLE V
COMPARISON OF AVERAGE MOTOR SPEED RESPONSE AND TORQUE RIPPLE UNDER PARAMETER INCREASE

Parameter mismatch	Control strategy	Speed response (s)	Torque ripple (N·m)
R=1.5R_s, ψ_f=1.5ψ_{f0}	MPCC-CFAPSO	0.0198	1.1035
	MPCC-DSCPSO	0.0169	1.0827
	RMPCC-ICAPSO	0.0152	1.0472
R=1.5R_s, ψ_f=1.5ψ_{f0}, L_s=1.5L_s	MPCC-CFAPSO	0.0201	1.2138
	MPCC-DSCPSO	0.0175	1.1439
	RMPCC-ICAPSO	0.0149	1.0253

reduced by 21.79% compared to MPCC-CFAPSO and 19.29% compared to the MPCC-DSCPSO.

In case of $R = 0.5R_s$, $\psi_f = 0.5\psi_{f0}$, and $L_s = 0.5L_s$, the average speed response of RMPCC-ICAPSO is 0.0158 s and the average torque ripple is 0.8409 N·m. The average speed response of RMPCC-ICAPSO is improved by 22.55% compared to the MPCC-CFAPSO and improved by 8.67% compared to

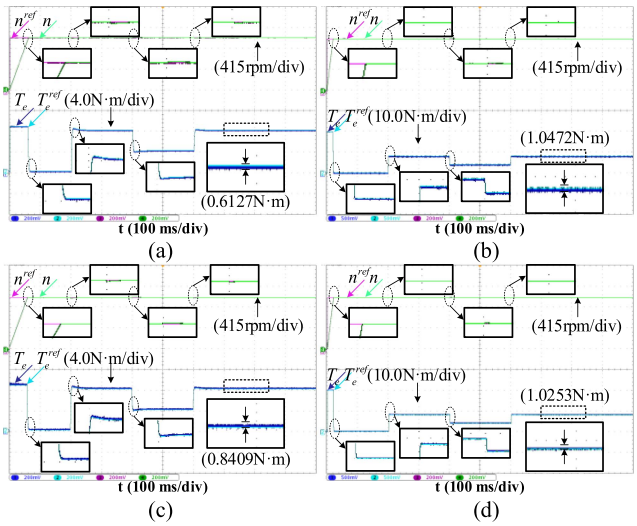

Fig. 15. Performance of the speed ω_e and torque T_e for the proposed RMPCC-ICAPSO strategy. (a) $R = 0.5R_s$ and $\psi_f = 0.5\psi_{f0}$. (b) $R = 1.5R_s$ and $\psi_f = 1.5\psi_{f0}$. (c) $R = 0.5R_s$, $\psi_f = 0.5\psi_{f0}$, and $L_s = 0.5L_{s0}$. (d) $R = 1.5R_s$, $\psi_f = 1.5\psi_{f0}$, and $L_s = 1.5L_{s0}$.

the MPCC-DSCPSO. The average torque ripple of RMPCC-ICAPSO is reduced by 25.43% compared to MPCC-CFAPSO and 23.98% compared to the MPCC-DSCPSO.

In case of $R = 1.5R_s$ and $\psi_f = 1.5\psi_{f0}$, the average speed response of RMPCC-ICAPSO is 0.0152 s and the average torque ripple is 1.0472 N·m. The average speed response of RMPCC-ICAPSO is improved by 23.23% compared to the MPCC-CFAPSO and improved by 10.06% compared to the MPCC-DSCPSO. The average torque ripple of RMPCC-ICAPSO is reduced by 5.10% compared to MPCC-CFAPSO and 3.28% compared to the MPCC-DSCPSO.

In case of $R = 1.5R_s$, $\psi_f = 1.5\psi_{f0}$, and $L_s = 1.5L_s$, the average speed response of RMPCC-ICAPSO is 0.0149 s, and the average torque ripple is 1.0253 N·m. The average speed response of RMPCC-ICAPSO is improved by 25.87% compared to the MPCC-CFAPSO and improved by 14.86% compared to the MPCC-DSCPSO. The average torque ripple of RMPCC-ICAPSO is reduced by 15.53% compared to MPCC-CFAPSO and 10.37% compared to the MPCC-DSCPSO.

C. Analysis of Estimation Results Under the Mismatch of Motor Parameters

To validate the parameter estimation performance of the RMPCC-ICAPSO strategy, it is compared with the MPCC-CFAPSO strategy in [28] and the MPCC-DSCPSO strategy in [36] under various parameters. The estimation results as the parameters are reduced to 0.5 times the rated value are shown in Table VI. The estimation results as the parameters are increased to 1.5 times the rated value are shown in Table VII.

The estimation results of R_s are shown in Fig. 16. In Fig. 16(a), $R = 0.5R_s$. The estimation R_s of the RMPCC-ICAPSO is 0.1114 Ω, estimation time is 0.0095 s, and estimation error is 1.2727%. The estimation time of RMPCC-ICAPSO is reduced by 33.09% compared to MPCC-CFAPSO and 25.78% compared

TABLE VI
ESTIMATION RESULTS AS THE PARAMETERS ARE REDUCED TO 0.5 TIMES OF THE RATED VALUE

Parameter	MPCC-CFAPSO	MPCC-DSCPSO	RMPCC-ICAPSO
R_s (Ω)	0.1124	0.1079	0.1114
Estimate time (s)	0.0142	0.0128	0.0095
Error (%)	2.1818	1.9091	1.2727
L_s (mH)	0.7996	0.8213	0.8194
Estimate time (s)	0.0179	0.0172	0.0158
Error (%)	1.5877	1.0831	0.8492
Ψ_f (Wb)	0.0509	0.0494	0.0496
Estimate time (s)	0.0164	0.0125	0.0102
Error (%)	1.8000	1.2000	0.8000

TABLE VII
ESTIMATION RESULTS AS THE PARAMETERS ARE INCREASED TO 1.5 TIMES OF THE RATED VALUE

Parameter	MPCC-CFAPSO	MPCC-DSCPSO	RMPCC-ICAPSO
R_s (Ω)	0.3378	0.3233	0.3345
Estimate time (s)	0.0298	0.0275	0.0208
Error (%)	2.3636	2.0303	1.3636
L_s (mH)	2.3937	2.4651	2.4587
Estimate time (s)	0.0382	0.0351	0.0302
Error (%)	1.7969	1.1323	0.8697
Ψ_f (Wb)	0.1528	0.1480	0.1486
Estimate time (s)	0.0348	0.0312	0.0209
Error (%)	1.8667	1.3333	0.9333

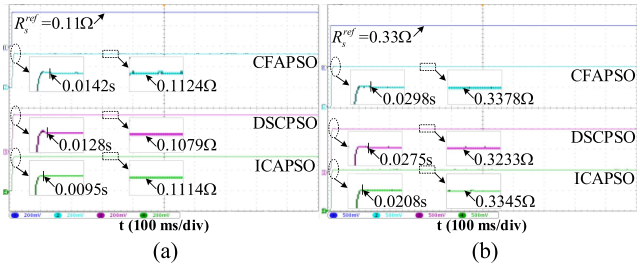

Fig. 16. Results of the resistance estimation. (a) $R = 0.5R_s$. (b) $R = 1.5R_s$.

to MPCC-DSCPSO. The estimation error of RMPCC-ICAPSO is reduced by 41.67% compared to MPCC-CFAPSO and 33.34% compared to MPCC-DSCPSO. In Fig. 16(b), $R = 1.5R_s$. The estimation R_s of RMPCC-ICAPSO is 0.3345 Ω, estimation time is 0.0208 s, and estimation error is 1.3636%. The estimation time of RMPCC-ICAPSO is reduced by 30.20% compared to MPCC-CFAPSO and 24.36% compared to MPCC-DSCPSO. The estimation error of RMPCC-ICAPSO is reduced by 42.31% compared to MPCC-CFAPSO and 32.84% compared to MPCC-DSCPSO.

The estimation results of L_s are shown in Fig. 17. In Fig. 17(a), $L_s = 0.5L_{s0}$. The estimation L_s of the RMPCC-ICAPSO is 0.8194 mH, estimation time is 0.0158 s, and estimation error is 0.8492%. The estimation time of RMPCC-ICAPSO is reduced by 11.73% compared to MPCC-CFAPSO and 8.14% compared to MPCC-DSCPSO. The estimation error of RMPCC-ICAPSO is reduced by 46.51% compared to MPCC-CFAPSO and 21.59%

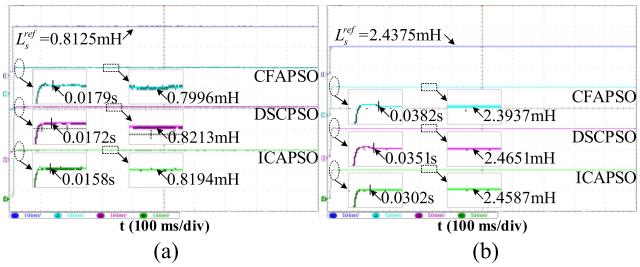

Fig. 17. Results of the inductance estimation. (a) $L_s = 0.5L_{s0}$. (b) $L_s = 1.5L_{s0}$.

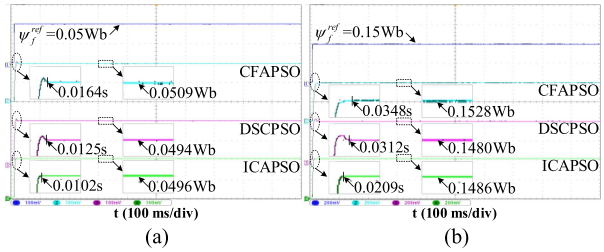

Fig. 18. Results of the flux linkage estimation. (a) $\psi_f = 0.5\psi_{f0}$. (b) $\psi_f = 1.5\psi_{f0}$.

compared to MPCC-DSCPSO. In Fig. 17(b), $L_s = 1.5L_{s0}$. The estimation L_s of the RMPCC-ICAPSO is 2.4587 mH, estimation time is 0.0302 s, and estimation error is 0.8697%. The estimation time of RMPCC-ICAPSO is reduced by 20.94% compared to MPCC-CFAPSO and 13.96% compared to MPCC-DSCPSO. The estimation error of RMPCC-ICAPSO is reduced by 51.59% compared to MPCC-CFAPSO and 23.19% compared to MPCC-DSCPSO.

The estimation results of ψ_f are shown in Fig. 18. In Fig. 18(a), $\psi_f = 0.5\psi_{f0}$. The estimation ψ_f of the proposed RMPCC-ICAPSO is 0.0496 Wb, estimation time is 0.0102 s, and estimation error is 0.8%. The estimation time of RMPCC-ICAPSO is reduced by 37.81% compared to MPCC-CFAPSO and 18.4% compared to MPCC-DSCPSO. The estimation error of RMPCC-ICAPSO is reduced by 55.56% compared to MPCC-CFAPSO and 33.33% compared to MPCC-DSCPSO. In Fig. 18(b), $\psi_f = 1.5\psi_{f0}$. The estimation ψ_f of the RMPCC-ICAPSO is 0.1486 Wb, estimation time is 0.0209 s, and estimation error is 0.9333%. The estimation time of RMPCC-ICAPSO is reduced by 39.94% compared to MPCC-CFAPSO and 33.01% compared to MPCC-DSCPSO. The estimation error of the RMPCC-ICAPSO is reduced by 50.0% compared to MPCC-CFAPSO and 30.0% compared to the MPCC-DSCPSO.

D. Harmonic Analysis of the Stator Current

The experimental waveforms of stator current under the parameter mismatch condition are shown in Figs. 19–21. The analysis of peak value current and total harmonic distortion (THD) of stator current for parameter mismatch conditions are shown in Table VIII.

As the motor operating conditions are set to $R = 0.5R_s$ and $\psi_f = 0.5\psi_{f0}$, the THD of i_a is 4.13% for the MPCC-CFAPSO, 3.52% for the MPCC-DSCPSO, and 2.65% for the proposed RMPCC-ICAPSO strategy. The stator current THD of the RMPCC-ICAPSO is reduced by 35.84% compared to MPCC-CFAPSO and 24.72% compared to MPCC-DSCPSO.

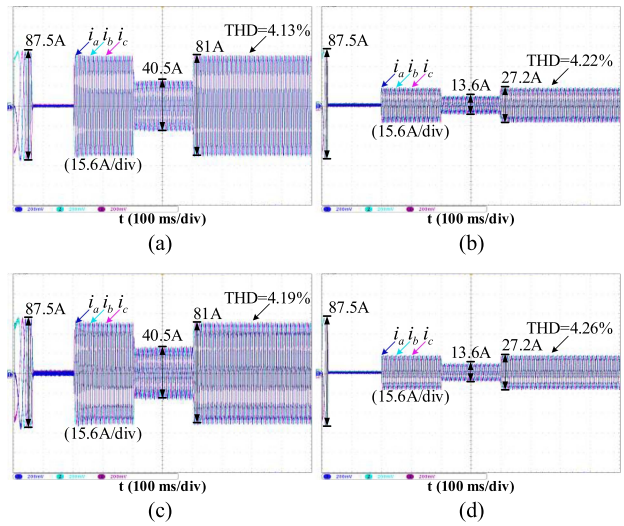

Fig. 19. Performance of stator current for the MPCC-CFAPSO strategy in [28]. (a) $R = 0.5R_s$ and $\psi_f = 0.5\psi_{f0}$. (b) $R = 1.5R_s$ and $\psi_f = 1.5\psi_{f0}$. (c) $R = 0.5R_s$, $\psi_f = 0.5\psi_{f0}$, and $L_s = 0.5L_{s0}$. (d) $R = 1.5R_s$, $\psi_f = 1.5\psi_{f0}$, and $L_s = 1.5L_{s0}$.

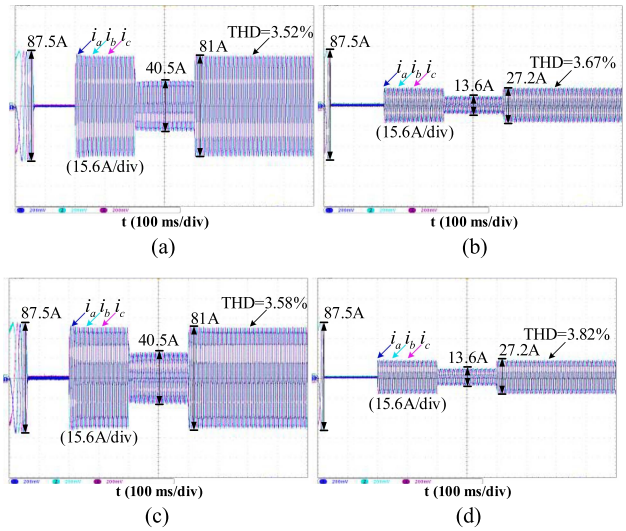

Fig. 20. Performance of stator current for the MPCC-DSCPSO strategy in [36]. (a) $R = 0.5R_s$ and $\psi_f = 0.5\psi_{f0}$. (b) $R = 1.5R_s$ and $\psi_f = 1.5\psi_{f0}$. (c) $R = 0.5R_s$, $\psi_f = 0.5\psi_{f0}$, and $L_s = 0.5L_{s0}$. (d) $R = 1.5R_s$, $\psi_f = 1.5\psi_{f0}$, and $L_s = 1.5L_{s0}$.

As the motor operating conditions are set to $R = 1.5R_s$ and $\psi_f = 1.5\psi_{f0}$, the THD of i_a is 4.22% for the MPCC-CFAPSO, 3.67% for the MPCC-DSCPSO, and 2.78% for the proposed RMPCC-ICAPSO strategy. The stator current THD of the RMPCC-ICAPSO is reduced by 34.12% compared to MPCC-CFAPSO and 24.25% compared to MPCC-DSCPSO.

As the motor operating conditions are set to $R = 0.5R_s$, $\psi_f = 0.5\psi_{f0}$, and $L_s = 0.5L_s$, the THD of i_a is 4.19% for the MPCC-CFAPSO, 3.58% for the MPCC-DSCPSO, and 2.73% for the proposed RMPCC-ICAPSO. The stator current THD

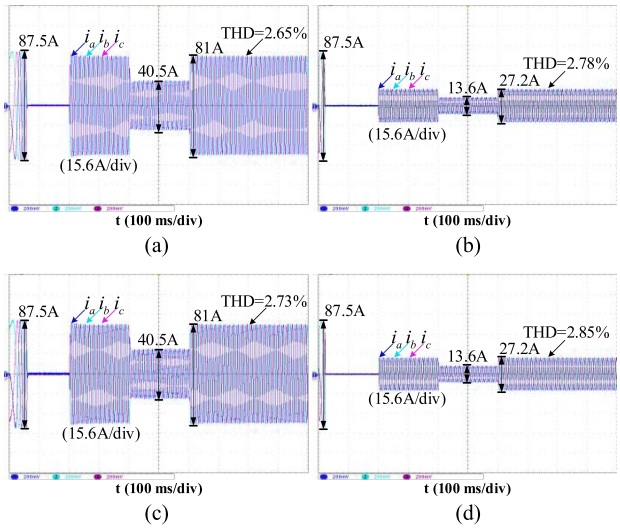

Fig. 21. Performance of stator current for the proposed RMPCC-ICAPSO strategy. (a) $R = 0.5R_s$ and $\psi_f = 0.5\psi_{f0}$. (b) $R = 1.5R_s$ and $\psi_f = 1.5\psi_{f0}$. (c) $R = 0.5R_s$, $\psi_f = 0.5\psi_{f0}$, and $L_s = 0.5L_{s0}$. (d) $R = 1.5R_s$, $\psi_f = 1.5\psi_{f0}$, and $L_s = 1.5L_{s0}$.

TABLE VIII
ANALYSIS OF PEAK VALUE AND THD OF STATOR CURRENT FOR PARAMETER MISMATCH CONDITIONS

Parameter mismatch	Control strategy	Peak value of stator current (A)	THD(%)
R=0.5R_s, ψ_f=0.5ψ_{f0}	MPCC-CFAPSO	40.526	4.13
	MPCC-DSCPSO	40.513	3.52
	RMPCC-ICAPSO	40.509	2.65
R=1.5R_s, ψ_f=1.5ψ_{f0}	MPCC-CFAPSO	13.573	4.22
	MPCC-DSCPSO	13.578	3.67
	RMPCC-ICAPSO	13.582	2.78
R=0.5R_s, ψ_f=0.5ψ_{f0}, L_s=0.5L_s	MPCC-CFAPSO	40.537	4.19
	MPCC-DSCPSO	40.519	3.58
	RMPCC-ICAPSO	40.511	2.73
R=1.5R_s, ψ_f=1.5ψ_{f0}, L_s=1.5L_s	MPCC-CFAPSO	13.569	4.26
	MPCC-DSCPSO	13.574	3.82
	RMPCC-ICAPSO	13.586	2.85

of the RMPCC-ICAPSO is reduced by 34.85% compared to MPCC-CFAPSO and 23.74% compared to MPCC-DSCPSO.

As the motor operating conditions are set to $R = 1.5R_s$, $\psi_f = 1.5\psi_{f0}$, and $L_s = 1.5L_s$, the THD of i_a is 4.26% for the MPCC-CFAPSO, 3.82% for the MPCC-DSCPSO, and 2.85% for the proposed RMPCC-ICAPSO. The stator current THD of the RMPCC-ICAPSO is reduced by 33.09% compared to MPCC-CFAPSO and 25.39% compared to MPCC-DSCPSO.

E. Analysis of Code Execution Time and Prediction Counts

The proposed RMPCC strategy uses fixed voltage vectors u_1 and u_3 to design the control algorithm without traversal of the cost function for optimization. The control structure is simplified as the three-phase duty cycle is reconstructed and corrected to act directly on the inverter. The antipredator behavior is introduced into the particle swarm optimization algorithm, the convergence speed of particles is accelerated, and the identification ability is enhanced. The comparison of code execution time and prediction counts for the three strategies is shown in Table IX. The code execution time of the proposed RMPCC-ICAPSO is 53.2 μs, which is reduced by 3.97% compared to MPCC-CFAPSO and 18.03% compared to MPCC-DSCPSO. The proposed RMPCC-ICAPSO is better able to meet the requirements of a real-time motor system.

TABLE IX
COMPARISON OF CODE EXECUTION TIME AND PREDICTION COUNTS

Control strategy	Execution time	Prediction counts
MPCC-CFAPSO	55.4 μs	1
MPCC-DSCPSO	64.9 μs	1
RMPCC-ICAPSO	53.2 μs	1

VI. CONCLUSION

Aiming at the issues of the current fluctuation and high dependence of control performance on model parameters accuracy in the MPCC, a robust model predictive current closed-loop control with parameter estimation strategy based on immune chaotic antipredator PSO algorithm is proposed. According to the theoretical research and analysis of experimental results, the conclusions obtained are as follows.

1) Compared to the MPCC-CFAPSO and MPCC-DSCPSO, the proposed RMPCC-ICAPSO achieves the average reduction of q-axis current fluctuation by 27.69% and 15.93%, d-axis current fluctuation by 27.21% and 21.73%, and the average reduction of stator current THD by 34.48% and 24.53% under the parameter mismatch condition.
2) Compared to the MPCC-CFAPSO and MPCC-DSCPSO, the proposed RMPCC-ICAPSO achieves the average improvement of 24.01% and 10.87% in speed response and reduction of 16.96% and 14.23% in torque pulsation under the parameter mismatch condition.
3) Compared to the MPCC-CFAPSO and MPCC-DSCPSO, the proposed RMPCC-ICAPSO reduces the resistance estimation error by 41.99% and 33.09%, the inductance estimation error by 49.05% and 22.39%, and the flux linkage estimation error by 52.78% and 31.67% under the parameter mismatch condition.

REFERENCES

[1] X. Fang, S. Lin, X. Wang, Z. Yang, F. Lin, and Z. Tian, "Model predictive current control of traction permanent magnet synchronous motors in six-step operation for railway application," *IEEE Trans. Ind. Electron.*, vol. 69, no. 9, pp. 8751–8759, Sep. 2022.
[2] Z. Chen, T. Shi, Z. Lin, Z. Wang, and X. Gu, "Analysis and control of current harmonic in IPMSM field-oriented control system," *IEEE Trans. Power Electron.*, vol. 37, no. 8, pp. 9571–9585, Aug. 2022.
[3] S. Fang, Y. Wang, W. Wang, Y. Chen, and Y. Chen, "Design of permanent magnet synchronous motor servo system based on improved particle swarm optimization," *IEEE Trans. Power Electron.*, vol. 37, no. 5, pp. 5833–5846, May 2022.

[4] H. Lin, S. Niu, Z. Xue, and S. Wang, "A simplified virtual-vector-based model predictive control technique with a control factor for three-phase SPMSM drives," *IEEE Trans. Power Electron.*, vol. 38, no. 6, pp. 7546–7557, Jun. 2023.

[5] A. U. Rehman, H. H. Choi, and J.-W. Jung, "An optimal direct torque control strategy for surface-mounted permanent magnet synchronous motor drives," *IEEE Trans. Ind. Inform.*, vol. 17, no. 11, pp. 7390–7400, Nov. 2021.

[6] C. Xiong, T. Guan, P. Zhou, and H. Xu, "A fault-tolerant FOC strategy for five-phase SPMSM with minimum torque ripples in the full torque operation range under double-phase open-circuit fault," *IEEE Trans. Ind. Electron.*, vol. 67, no. 11, pp. 9059–9072, Nov. 2020.

[7] K. Zhang, M. Fan, Y. Yang, Z. Zhu, C. Garcia, and J. Rodriguez, "Field enhancing model predictive direct torque control of permanent magnet synchronous machine," *IEEE Trans. Energy Convers.*, vol. 36, no. 4, pp. 2924–2933, Dec. 2021.

[8] P. F. C. Gonçalves, S. M. A. Cruz, and A. M. S. Mendes, "Disturbance observer based predictive current control of six-phase permanent magnet synchronous machines for the mitigation of steady-state errors and current harmonics," *IEEE Trans. Ind. Electron.*, vol. 69, no. 1, pp. 130–140, Jan. 2022.

[9] Y. Zhang, D. Xu, J. Liu, S. Gao, and W. Xu, "Performance improvement of model-predictive current control of permanent magnet synchronous motor drives," *IEEE Trans. Ind. Appl.*, vol. 53, no. 4, pp. 3683–3695, Jul./Aug. 2017.

[10] X. Li, W. Tian, X. Gao, Q. Yang, and R. Kennel, "A generalized observer-based robust predictive current control strategy for PMSM drive system," *IEEE Trans. Ind. Electron.*, vol. 69, no. 2, pp. 1322–1332, Feb. 2022.

[11] X. Sun, Z. Jin, Y. Cai, Z. Yang, and L. Chen, "Grey wolf optimization algorithm-based state feedback control for a bearingless permanent magnet synchronous machine," *IEEE Trans. Power Electron.*, vol. 35, no. 12, pp. 13631–13640, Dec. 2020.

[12] Z.-H. Liu, H.-L. Wei, Q.-C. Zhong, K. Liu, X.-S. Xiao, and L.-H. Wu, "Parameter estimation for VSI-Fed PMSM based on a dynamic PSO with learning strategies," *IEEE Trans. Power Electron.*, vol. 32, no. 4, pp. 3154–3165, Apr. 2017.

[13] T. Li, X. Sun, G. Lei, Y. Guo, Z. Yang, and J. Zhu, "Finite-control-set model predictive control of permanent magnet synchronous motor drive systems—An overview," *IEEE/CAA J. Automatica Sinica*, vol. 9, no. 12, pp. 2087–2105, Dec. 2022.

[14] X. Zhang and Z. Liu, "Robustness optimization of model predictive current control for PMSM drives considering dynamic response influence," *IEEE J. Emerg. Sel. Topics Ind. Electron.*, vol. 4, no. 2, pp. 678–687, Apr. 2023.

[15] X. Zhang, L. Zhang, and Y. Zhang, "Model predictive current control for PMSM drives with parameter robustness improvement," *IEEE Trans. Power Electron.*, vol. 34, no. 2, pp. 1645–1657, Feb. 2019.

[16] Y. Han, C. Gong, L. Yan, H. Wen, Y. Wang, and K. Shen, "Multiobjective finite control set model predictive control using novel delay compensation technique for PMSM," *IEEE Trans. Power Electron.*, vol. 35, no. 10, pp. 11193–11204, Oct. 2020.

[17] X. Zhang, Z. Zhao, Y. Cheng, and Y. Wang, "Robust model predictive current control based on inductance and flux linkage extraction algorithm," *IEEE Trans. Veh. Technol.*, vol. 69, no. 12, pp. 14893–14902, Dec. 2020.

[18] X. Song, H. Wang, X. Ma, X. Yuan, and X. Wu, "Robust model predictive current control for a nine-phase open-end winding PMSM with high computational efficiency," *IEEE Trans. Power Electron.*, vol. 38, no. 11, pp. 13933–13943, Nov. 2023.

[19] H. Liu, W. Lin, Z. Liu, C. Buccella, and C. Cecati, "Model predictive current control with model-aid extended state observer compensation for PMSM drive," *IEEE Trans. Power Electron.*, vol. 38, no. 3, pp. 3152–3162, Mar. 2023.

[20] X. Guo et al., "An improved integral sliding mode control for PMSM drives based on new variable rate reaching law with adaptive reduced-order PI observer," *IEEE Trans. Transport. Electrific.*, vol. 9, no. 3, pp. 4503–4516, Sep. 2023.

[21] L. Qu, W. Qiao, and L. Qu, "Active-disturbance-rejection-based sliding-mode current control for permanent-magnet synchronous motors," *IEEE Trans. Power Electron.*, vol. 36, no. 1, pp. 751–760, Jan. 2021.

[22] X. An, G. Liu, Q. Chen, W. Zhao, and X. Song, "Adjustable model predictive control for IPMSM drives based on online stator inductance identification," *IEEE Trans. Ind. Electron.*, vol. 69, no. 4, pp. 3368–3381, Apr. 2022.

[23] A. Brosch, O. Wallscheid, and J. Böcker, "Long-term memory recursive least squares online identification of highly utilized permanent magnet synchronous motors for finite-control-set model predictive control," *IEEE Trans. Power Electron.*, vol. 38, no. 2, pp. 1451–1467, Feb. 2023.

[24] F. Wang et al., "Design of model predictive control weighting factors for PMSM using Gaussian distribution-based particle swarm optimization," *IEEE Trans. Ind. Electron.*, vol. 69, no. 11, pp. 10935–10946, Nov. 2022.

[25] H. Li, J. Shao, and Z. Liu, "Incremental model predictive current control for PMSM with online compensation for parameter mismatch," *IEEE Trans. Energy Convers.*, vol. 38, no. 2, pp. 1050–1059, Jun. 2023.

[26] Y. Wang et al., "A robust DPCC for IPMSM based on a full parameter identification method," *IEEE Trans. Ind. Electron.*, vol. 70, no. 8, pp. 7695–7705, Aug. 2023.

[27] Y. Wang, Y. Xu, and J. Zou, "Online multiparameter identification method for sensorless control of SPMSM," *IEEE Trans. Power Electron.*, vol. 35, no. 10, pp. 10601–10613, Oct. 2020.

[28] Y. Zhang, M. Zhou, C. Zhang, A. Shen, and L. Bing, "Identification of PMSM parameters with time-error compensated based on contractile factor antipredator PSO," *IEEE Trans. Transport. Electrific.*, vol. 10, no. 2, pp. 4006–4017, Jun. 2024.

[29] K. K. Prabhakaran and A. Karthikeyan, "Electromagnetic torque-based model reference adaptive system speed estimator for sensorless surface mount permanent magnet synchronous motor drive," *IEEE Trans. Ind. Electron.*, vol. 67, no. 7, pp. 5936–5947, Jul. 2020.

[30] Z. Wu, K. Ding, Z. Yang, and G. He, "Analytical prediction and minimization of deadtime-related harmonics in permanent magnet synchronous motor," *IEEE Trans. Ind. Electron.*, vol. 68, no. 9, pp. 7736–7746, Sep. 2021.

[31] H. T. Nguyen and J.-W. Jung, "Finite control set model predictive control to guarantee stability and robustness for surface-mounted PM synchronous motors," *IEEE Trans. Ind. Electron.*, vol. 65, no. 11, pp. 8510–8519, Nov. 2018.

[32] X. Liu, L. Zhou, J. Wang, X. Gao, Z. Li, and Z. Zhang, "Robust predictive current control of permanent-magnet synchronous motors with newly designed cost function," *IEEE Trans. Power Electron.*, vol. 35, no. 10, pp. 10778–10788, Oct. 2020.

[33] Z. Li, F. Wang, D. Ke, J. Li, and W. Zhang, "Robust continuous model predictive speed and current control for PMSM with adaptive integral sliding-mode approach," *IEEE Trans. Power Electron.*, vol. 36, no. 12, pp. 14398–14408, Dec. 2021.

[34] A. Brosch, S. Hanke, O. Wallscheid, and J. Böcker, "Data-driven recursive least squares estimation for model predictive current control of permanent magnet synchronous motors," *IEEE Trans. Power Electron.*, vol. 36, no. 2, pp. 2179–2190, Feb. 2021.

[35] Q. Wang, G. Wang, N. Zhao, G. Zhang, Q. Cui, and D. Xu, "An impedance model-based multiparameter identification method of PMSM for both offline and online conditions," *IEEE Trans. Power Electron.*, vol. 36, no. 1, pp. 727–738, Jan. 2021.

[36] W. Feng, W. Zhang, and S. Huang, "A novel parameter estimation method for PMSM by using chaotic particle swarm optimization with dynamic self-optimization," *IEEE Trans. Veh. Technol.*, vol. 72, no. 7, pp. 8424–8432, Jul. 2023.